Effect of Metal Nanoparticle Aggregate Structure on the Thermodynamics of Oxidative Dissolution

Dhruba K. Pattadar,[a],† Harikrishnan N. Nambiar,[b],† Stacy L. Allen,[b] Jacek B. Jasinski[c] and Francis P. Zamborini[b],*

[a]Department of Chemistry and Biochemistry, University of Arizona, Tucson, Arizona 85721-0041, United States

[b]Department of Chemistry and [c]Conn Center for Renewable Energy Research, University of Louisville, Louisville, Kentucky 40292, United States

* Corresponding Author, Email: f.zamborini@louisville.edu

† These two authors contributed equally.

ABSTRACT

Here we compare the electrochemical oxidation potential of 15 nm diameter citrate-stabilized Au NPs aggregated by acid (low pH) to those aggregated by tetrakis(hydroxymethyl) phosphonium chloride (THPC). For acid-induced aggregation, the solution changes to a blue-violet color, the localized surface plasmon resonance (LSPR) band of the Au NPs at 520 nm decreases along with an increase in absorbance at higher wavelengths (600-800 nm), and the peak oxidation potential (E_p) in anodic stripping voltammetry (ASV) obtained in bromide shifts positive by as large as 200 mV. For THPC-induced aggregation (Au:THPC mole ratio = 62.5), the solution changes to a blue color as the LSPR band at 520 nm decreases and a new distinct peak at 700 nm appears, but the E_p does not shift positive. Scanning transmission electron microscopy (STEM) images reveal that the acid-induced aggregates are three-dimensional with strongly-fused Au NP-Au NP contacts while the THPC-induced aggregates are linear or two-dimensional with ~1 nm separation between Au NPs. The surface area-to-volume ratio (SA/V) decreases for the acid

aggregated Au NPs due to strong Au NP-Au NP contacts, which leads to lower surface free energy and a higher E_p. The SA/V does not change for the THPC-aggregated Au NPs since space remains between them and their SA is fully accessible. These findings show that metal NP oxidative stability, as determined by ASV, is highly sensitive to the details of the aggregate structure.

INTRODUCTION

The aggregation of metal nanoparticles (NPs) involves the clumping together, or coagulation, of NPs in solution. This occurs upon destabilization of the dispersed NPs, which are usually stabilized by capping agents, such as polymers,[1] surfactants,[2] ions,[3] or ligands attached to the NP surface.[4] These capping agents, or stabilizers, control the size and shape of NPs during synthesis and also prevent aggregation of the NPs. Aggregation is widely considered a bad situation, leading to NP destabilization and eventual precipitation, rendering the NPs useless for many applications.[5-6] Aggregation can lead to NP catalyst deactivation, for example.[5, 7] On the other hand, the aggregation of metal NPs is often part of the synthesis process and can be exploited for useful applications. For example, the aggregation of metal NPs can be controlled to occur in the presence of some analyte of interest, serving as a means to detect the analyte.[8-11] Due to the plasmonic properties of Au and Ag NPs in the visible range, for example, the aggregation of these metal NPs leads to plasmonic coupling, resulting in a change in color due to a change in the absorbance wavelength of the localized surface plasmon resonance (LSPR) band. For example, two different types of ss-DNA-functionalized Au NPs become aggregated in the presence of a complementary ss-DNA target analyte in solution.[11-12] This leads to a noticeable color change that provides a positive signal that the analyte of interest is present in solution. In addition, the aggregation of metal NPs can be exploited for improving the scattering intensity in surface-enhanced Raman

spectroscopy (SERS).[13-15] SERS measurements for molecules located in between aggregated metal NPs allow single molecule detection due to this enhanced signal.

Controlled aggregation has also been exploited to create materials with catalytic switching behavior, which is based on the loss in catalytic activity in the aggregated state and high catalytic activity in the dispersed (non-aggregated) state. For example, Wei and coworkers reported on a photo-switchable hydrosilylation reaction mediated by dynamic aggregation of Au NPs.[16] Others used aggregated NPs for electrocatalytic oxidation of methanol,[17] glucose,[18] and ethanol.[19] While much less common, catalytic activity has in some cases increased with metal NPs in the aggregated state. For example, Wen and coworkers showed that the electrocatalytic glucose oxidation reactivity increased for a dopamine induced, aggregated 5-6 nm diameter Au aerogel synthesized with beta-cyclodextrin as compared to citrate-stabilized isolated NPs of a similar size.[18] The increased reactivity was thought to be caused by the increase in conductivity, porosity, electron transfer kinetics, and mass transport at the high surface area aggregated NPs. Finally, superstructures of metal NPs assembled by controlled aggregation have found various applications in nanoelectronics or as plasmonic waveguides. Considering NP stability and all the situations that depend on NP aggregation (optical sensing, SERS, catalysis, devices), aggregation is clearly an issue of great importance in NP research.

It is clearly necessary to develop techniques for detecting the aggregation of metal NPs. Aggregation has mainly been studied by optical methods, such as UV-vis spectroscopy[20] and dynamic light scattering (DLS),[21] and imaging methods, such as scanning probe microscopy,[22] scanning electron microscopy (SEM),[23] and transmission electron microscopy (TEM).[5] There are much fewer studies on the electrochemical monitoring of the aggregation of metal NPs. Some studies have observed the effect of aggregation on metal NP oxidation current,[24-27] while Allen *et*

al. were the first to show a positive shift in the peak oxidation potential (E_p) upon Au NP aggregation.[23] The aggregation of citrate-stabilized Au NPs was first controlled in solution by adding acid (lowering the pH). Then, the NPs were attached to a glass/ITO electrode and characterized electrochemically by anodic stripping voltammetry (ASV). It was found that after aggregation,[23] the overall surface area-to-volume ratio (SA/V) of the Au NPs decreased dramatically, leading to lower surface free energy and a positive shift in E_p. Others have detected metal NP aggregation for assemblies or single metal NP collisions at microelectrodes by monitoring the overall current or the charge under the current spikes that result from NP collisions.[24, 26] The latter allows detection of the aggregate and an estimation of the aggregate number.[28]

Here we focus on the electrochemical oxidation behavior of 15 nm diameter citrate-stabilized Au NPs aggregated by adding acid as compared to those aggregated by adding tetrakis(hydroxymethyl) phosphonium chloride (THPC). These studies are important for several reasons. First, it is fundamentally important to know how different types of NP assemblies (or aggregates) change their SA/V ratio and E_p. Acid-aggregated and THPC-aggregated Au NPs result in very different assemblies with different NP-NP contacts and morphology. It is important to determine if the E_p of the NPs is affected by the NP-NP contact or aggregate morphology. Does the E_p depend on the details of the morphology and NP spacing in the aggregate, the overall SA/V of the Au NPs, or the extent of plasmonic coupling between Au NPs in the aggregated assembly? Importantly, monitoring the aggregation behavior of metal NPs by electrochemical methods is interesting fundamentally and could also be useful for sensing applications. We believe it will be more sensitive than optical and imaging methods and it does not require plasmonic NPs of a certain size. Towards the goal of developing electrochemical aggregation-based sensors, we demonstrate

here that ASV is highly sensitive to the aggregate structure and metal NP-NP contact arrangement in the aggregated assembly.

EXPERIMENTAL SECTION

Chemicals and Materials. (3-aminopropyl)triethoxysilane (≥ 98.0%), 2-propanol (ACS reagent) were purchased from Sigma Aldrich. $HAuCl_4 \cdot 3H_2O$ was synthesized from metallic Au (99.99%) in our lab. Acetone, methanol and ethyl alcohol (ACS/USP grade) were purchased from Pharmco-AAPER. Trisodium citrate salt, potassium perchlorate (99.0-100.5%), potassium bromide (GR ACS), and perchloric acid (60%) were purchased from Bio-Rad laboratories, Beantown Chemical, EMD, and Merck, respectively. Tetrakis(hydroxymethyl)phosphonium Chloride (80% solution in water) was purchased from ACROS ORGANICS. Indium-tin-oxide (ITO)-coated glass slides (CG-50IN-CUV, R_s = 8-12 Ω) were purchased from Delta Technologies Limited (Loveland, CO).

Synthesis of 15 nm Average Diameter Citrate-Stabilized Au NPs. 15 nm average diameter Au NPs were synthesized by a modified Turkevich method.[29] Briefly, 500 μL of 0.01 M $HAuCl_4 \cdot 3H_2O$ was added to 17.0 mL of nanopure water and heated to boiling. Immediately after boiling, 2.5 mL of 0.01 M citric acid, trisodium salt solution was added and the solution was stirred for 10 minutes. After 10 min, the solution turned to a bright red color indicating the formation of Au NPs. Finally, the resulting solution was stirred for another 15 min at room temperature and allowed to cool prior to attachment to glass/ITO/APTES electrodes for electrochemical analysis.

Aggregation of 15 nm Average Diameter Au NPs with THPC. Aggregation of Au NPs with THPC was obtained by the method reported by Gulka *et al.*.[30] Briefly, we added 1 μL of 100

μM, 400 μM, 600 μM and 1 mM THPC to the 5 mL aqueous solution of citrate-stabilized 15 nm diameter Au NPs, which gave Au:THPC mole ratios of 62.5, 31.3, 10.4 and 6.3, where the moles of Au refers to total Au atoms as opposed to Au NPs. Immediately after addition of THPC, the color of the Au NP solution changed from red to blue, indicating that the NPs were aggregated in solution. The aggregated Au NPs were immediately attached to a glass/ITO/APTES electrode by soaking for 3-5 min and then analyzed electrochemically.

Aggregation of 15 nm Average Diameter Au NPs with Acid. The pH of the solution of 15 nm diameter citrate-stabilized Au NPs was lowered by adding 10 μL of 8 M perchloric acid solution. After addition of acid, the color of the Au NP solution immediately turned to blue. The aggregated Au NPs were attached to a glass/ITO/APTES electrode by soaking the solution in the electrode for 4 to 5 minutes prior to electrochemical analysis.

Electrochemical Characterization. All electrochemical measurements were made with a CH Instruments model CHI 660E electrochemical workstation (Austin, TX). The working electrode was indium tin oxide-coated glass (glass/ITO) functionalized with (3-aminopropyl)triethoxysilane (APTES) as described by our group previously.[31-32] The isolated and aggregated 15 nm Au NPs were attached to the glass/ITO/APTES electrodes by soaking the electrodes in the appropriate solution for 3-5 minutes. A Pt wire counter electrode and an Ag/AgCl (3 M KCl) reference electrode completed the 3-electrode cell set up. Anodic stripping voltammetry (ASV) was performed by operating the instrument in linear sweep voltammetry (LSV) mode and scanning from -0.2 V to 1.4 V at a scan rate of 10 mV/s in 0.1 M $KClO_4$ plus 0.01 M KBr solution. The peak oxidation potential (E_p), due to Au oxidation to $AuBr_2^-$ or $AuBr_4^-$, was used for qualitative size determination and for monitoring the aggregation of the Au NPs. The integrated peak area from the ASV provides the Coulombs of charge passed during the complete oxidation (stripping)

of the Au NPs, which provides a measure of the total amount of Au on the electrode surface and is an indicator of the total volume (V) of the Au NPs on the electrode. To electrochemically measure the average surface area-to-volume ratio (SA/V) of the Au NPs on the electrode, cyclic voltammograms (CVs) were obtained in 0.1 M $HClO_4$ solution from -0.2 V to 1.6 V at a scan rate of 0.1 V/s. This leads to surface Au oxidation to Au_2O_3 at potentials above about 1.2 V and reduction of the Au_2O_3 back to Au on the reverse scan at about 0.8 V. The integrated area of the reduction peak provides the number of Coulombs passed during the reduction of Au_2O_3, serving as an indicator of the total electrochemically-exposed SA of the Au NPs on the electrode surface since Au oxide formation is a surface phenomenon. The SA/V ratio was obtained by dividing the Coulombs of charge obtained from the CV by the Coulombs of charge obtained from the ASV as described previously.[33] CV measurements had to be made before ASV measurements because of the destructive nature of ASV.

UV-Vis Characterization. Ultraviolet-visible spectrophotometry (UV-Vis) was performed using a Varian instrument Cary 50 Bio-spectrophotometer. UV-Vis spectra were obtained from 300-900 nm at a fast scan rate in glass cells with a 1 cm path length using water as the blank in aqueous solutions of the 15 nm diameter citrate-stabilized Au NPs that were non-aggregated or aggregated by acid or THPC. UV-Vis spectra of isolated NPs were obtained after 30 min of synthesis and aggregated NPs were obtained immediately after the addition of acid or THPC.

Microscopic Characterization. Scanning electron microscopy (SEM) images of isolated and aggregated 15 nm diameter citrate-stabilized Au NPs were obtained directly on glass/ITO/APTES electrodes by using a Carl Zeiss SMT AG SUPRA 35VP field emission scanning electron microscope (FESEM) operating at an accelerating voltage of 15.00 kV using an in-lens ion annular secondary electron detector. Scanning transmission electron microscopy (STEM) images of acid-

and THPC-aggregated Au NPs were obtained by using a 200 kV FEI Tecnai F20 operating in STEM mode. To mimic the attachment to glass/ITO/APTES electrodes, we used a silicon oxide-coated Au TEM grid functionalized with APTES in the same manner that the glass/ITO was functionalized. The Au NPs were attached to the APTES-functionalized grids by soaking the grids in the appropriate NP solution for 4-5 min. After soaking, the grids were gently rinsed with water and dried under N_2 prior to STEM analysis.

RESULTS AND DISCUSSION

Scheme 1 shows the general experimental procedure involved in these studies. Step 1 illustrates the synthesis of citrate-coated 15 nm diameter Au NPs. We synthesized 15 nm diameter citrate-stabilized Au NPs by the Turkevich method,[29] where the initial pH of the solution was ~5.8. In step 2a we lowered the pH from 5.8 to 2.6 by adding 1 μL of concentrated perchloric acid in order to aggregate the NPs as described by Allen *et al.* previously.[23] In step 2b we added THPC (instead of acid) in a separate 15 nm Au NP solution in order to get 1D and 2D aggregated assemblies of NPs as previously described by Gulka *et al.*[30] In the case of acid aggregation, the carboxylic acid group of the citrate ligands

Scheme 1. General experimental procedure involved in these studies.

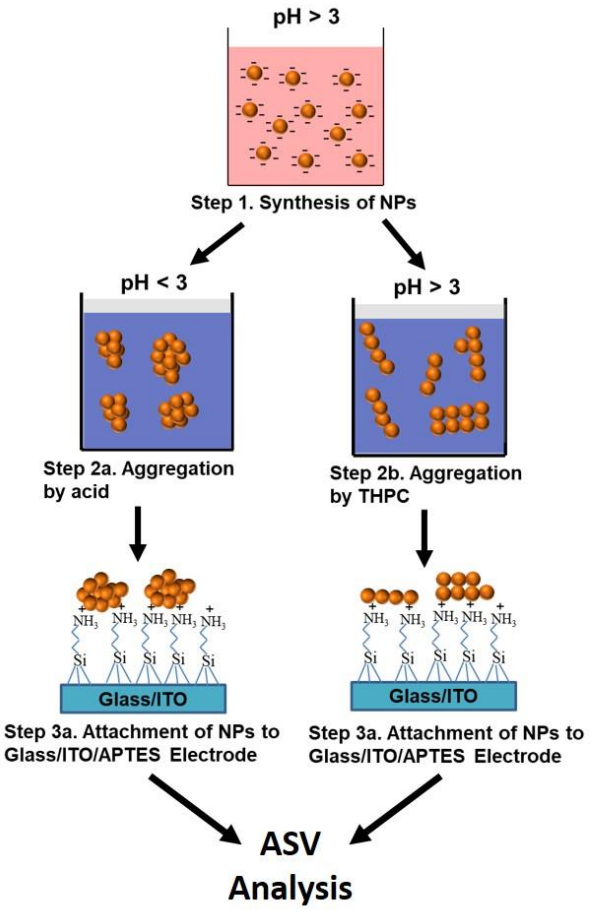

become protonated, which decreases the electrostatic repulsion between the NPs and ultimately the NPs become aggregated as reported by our group[23] and others.[34] However, in the case of THPC aggregation, it has been shown that THPC rapidly replaces citrate from the Au NP surfaces and produces a temporary dipole moment on each NP, which causes the NPs to form linear or 2D aggregated assemblies.[30, 35] Step 3 involves the attachment of the aggregated (acid or THPC) NPs to aminopropyltriethoxysilane-functionalized glass/ITO electrodes (glass/ITO/APTES) by directly soaking the functionalized electrodes in the aggregated (or non-aggregated for comparison) Au NP solutions.

Figure 1A shows UV-vis spectra of a solution of isolated, well-separated citrate-coated 15 nm diameter Au NPs (pH 5.8), acid-aggregated Au NPs (pH 2.6), and THPC-aggregated Au NPs (pH 5.8, Au:THPC mole ratio = 62.5). The localized surface plasmon resonance (LSPR) peak at 518 nm for the isolated, non-aggregated 15 nm Au NPs is consistent with that reported previously by our group[23] and others (Figure 1A, red plot).[36] The addition of acid to the 15 nm Au NPs to bring the pH to 2.6 caused the solution color to change from red to blue-violet immediately as shown in Figure S1 of supporting information. The UV-vis spectrum showed a slight red-shift of the peak from 518 to 523 nm, a decrease in the peak absorbance, and a significant increase of the baseline absorbance value at higher wavelengths (600-900 nm) as reported by our group previously (Figure 1A, black plot).[23] These well-known changes are due to plasmonic coupling between the connected Au NPs that occurs upon aggregation. The addition of THPC to the 15 nm Au NPs caused the color of the solution to immediately change from red to blue as shown in Figure S1 of supporting information. The LSPR band at 518 nm decreased significantly and a new, distinct LSPR band appeared at 710 nm (Figure 1A, blue plot). The color change and UV-vis of the 15

nm Au NPs after addition of acid and THPC showed clear aggregation in both cases, but there is a difference in them based on the different colors of the solution and difference in the UV-vis spectra at higher wavelengths (continuous absorbance from 600-900 nm versus distinct peak at 710 nm).

The corresponding anodic stripping voltammograms (ASVs) of the isolated and aggregated Au NPs attached to glass/ITO/APTES electrodes in 0.01 M KBr + 0.1 M $KClO_4$ are shown in Figure 1B. The ASV of the isolated Au NPs shows a single oxidation peak at 0.739 V vs Ag/AgCl (Figure 1B, red plot), which is consistent with our previous work.[37] The ASV of the acid-aggregated Au NPs shows the E_p at 0.951 V (Figure 1B, black plot), indicating that the NPs were aggregated in solution, consistent with the UV-vis spectrum (Figure 1A, black plot). Interestingly, the ASV of the THPC-aggregated NPs shows a single oxidation peak at 0.73 V (Figure 1B, blue plot), identical to the ASV of isolated Au NPs, even though the UV-vis spectrum and color change indicates that the particles were aggregated. This was puzzling since we expected the E_p to shift positive upon aggregation, similar to the acid-aggregated NPs.

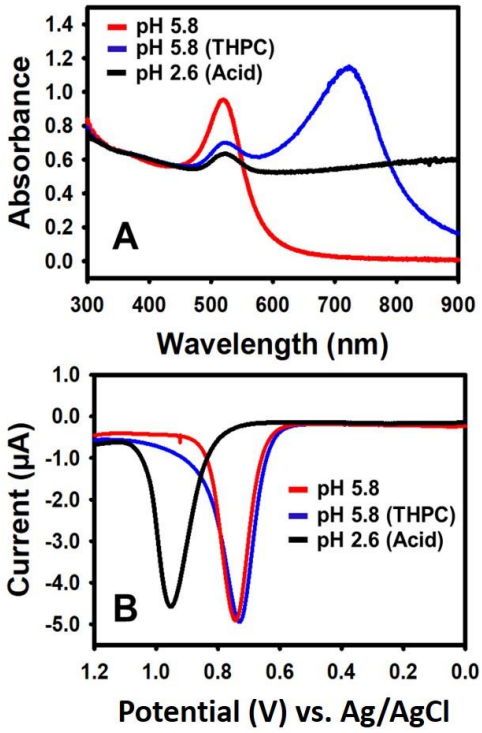

Figure 1. (A) UV−vis spectra of solutions of non-aggregated, isolated 15 nm diameter Au NPs at pH 5.8 (red graph), THPC-aggregated Au NPs at pH 5.8 (blue graph) and acid-aggregated Au NPs at pH 2.6 (black graph). (B) ASVs of glass/ITO/APTES electrodes after soaking in the solutions shown in (A). All ASVs were performed in 0.1 M $KClO_4$ + 0.01 M KBr from -0.2 to +1.4 V at a scan rate of 10 mV/s (only 0.0 to 1.2 V range is shown).

To better understand the reason for the different oxidation properties of the Au NPs aggregated by acid and THPC, we imaged them directly on the electrode surface by scanning electron microscopy (SEM). Figure 2A shows an SEM image of the non-aggregated 15 nm diameter citrate-stabilized Au NPs (pH 5.8) attached to a glass/ITO/APTES electrode, where they are clearly well-isolated. Figure 2B shows the same Au NPs after acid-aggregation by lowering the solution to pH 2.6. The Au NPs are clearly clumped together into fairly large three-dimensional (3D) aggregates, consistent with the color change in the UV-vis spectrum, and positive shift in the E_p in ASV. Figure 2C shows the same Au NPs aggregated with THPC. The Au NPs are also clumped together, but they are arranged into one-dimensional (1D) and two-dimensional (2D) aggregates. The 1D nature of the aggregates leads to the different color change and very distinct LSPR peak at 710 nm in the UV-vis spectrum, which is consistent with a longitudinal plasmon band observed in 1D arrays or 1D structures, such as wires or rods.[38-39] It is not very clear why the E_p did not shift positive with this type of aggregate structure though.

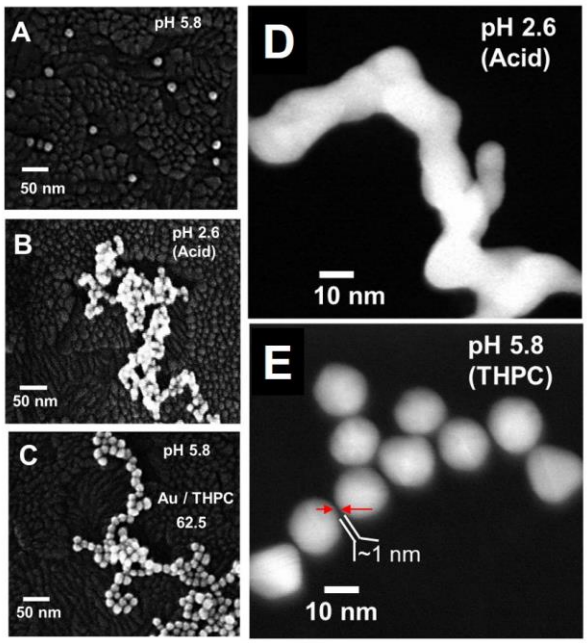

Figure 2. SEM images of glass/ITO/APTES electrodes coated with (A) non-aggregated 15 nm diameter citrate-coated Au NPs, (B) acid-aggregated 15 nm Au NPs, and (C) THPC-aggregated 15 nm Au NPs. Higher resolution STEM images of (D) acid-aggregated 15 nm Au NPs and (E) THPC-aggregated 15 nm Au NPs on APTES-functionalized silicon oxide-coated Au TEM grids.

The higher resolution STEM images of the acid aggregated and THPC-aggregated Au NPs in Figures 2D and 2E, respectively, provides more details about the aggregate structures. The acid-aggregated NPs have close Au NP-NP contacts and are fused together. In contrast, the THPC-

aggregated NPs show a clear ~1 nm space between the Au NPs in the 1D and 2D aggregates. Both types of aggregates lead to changes in plasmonic modes with the appearance of an aggregation band, but the different aggregates lead to different optical changes. The difference between the Au NP-Au NP contact is also the reason for the difference in the E_p, where the aggregates with 1 nm spacing behave very similar to well-isolated Au NPs (no shift in E_p), but the fused Au NP aggregates behave more like larger Au NPs with a more positive E_p. It is interesting that ASV can distinguish between these details in the aggregate structure.

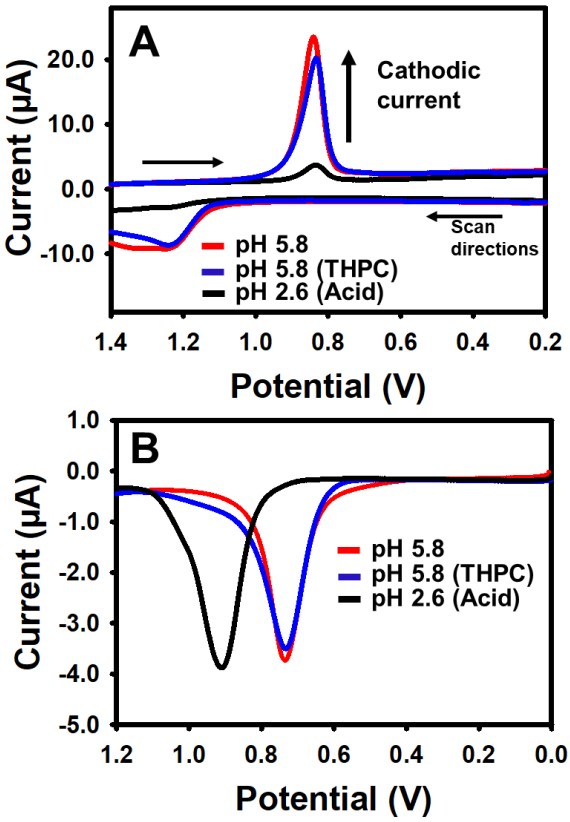

Figure 3. (A) CVs of glass/ITO/APTES electrodes soaked in solutions of non-aggregated 15 nm diameter Au NPs at pH 5.8 (red graph), THPC-aggregated 15 nm Au NPs (blue graph) and acid-aggregated Au NPs at pH 2.6 (black graph). CVs was performed in 0.1 M $HClO_4$ solution. (B) ASVs of the same electrodes as in (A) after the CV cycle was obtained. ASVs were performed in 0.1 M $KClO_4$ + 0.01 M KBr from -0.2 to +1.4 V at a scan rate of 10 mV/s (0.0 to 1.2 V is shown.)

We recently showed that the E_p of Au NPs ultimately depends on their SA/V.[40] This would explain the different E_p values of the two different aggregates. For acid-aggregated Au NPs, the close contact and fusion between NPs leads to a dramatically reduced SA/V, causing a positive shift in the E_p. For the THPC-aggregated Au NPs, the 1 nm spacing between the Au NPs allows full access of the SA, leading to a similar SA/V of the THPC-aggregated and non-aggregated, well-isolated Au NPs. This explains the E_p being the same for both. To confirm this, we electrochemically-measured the SA/V of the non-aggregated, acid-aggregated, and THPC-

aggregated Au NPs using our previously described procedure,[33, 41] which is briefly described in the experimental details in the supporting information. The total SA was measured by performing cyclic voltammetry (CV) of the Au NPs attached to glass/ITO/APTES in 0.1 M $HClO_4$ solution and the total volume of the same electrode was obtained from ASV in Br^--containing $KClO_4$ electrolyte solution. Figure 3A shows the CVs of non-aggregated (or isolated), THPC-aggregated, and acid-aggregated 15 nm diameter Au NPs. The peak area (in Coulombs) of the Au_2O_3 reduction peak at ~0.8 V is indicative of the total SA. Figure 3B shows ASVs of the non-aggregated, THPC-aggregated, and acid-aggregated Au NPs, where the peak area of the Au oxidation peak at 0.7 V or 0.9 V (in Coulombs) is indicative of the total V of Au. The peak areas of the Au oxidation peaks

Table 1. SA/V determination of isolated, acid-aggregated and THPC-aggregated 15 nm citrate-stabilized Au NPs.

Sample of Au NPs	Trial #	CV measured surface area (C)	ASV measured total volume (C)	Oxidation Peak potential E_p (V) vs Ag/AgCl	Surface area to total volume (SA/V)	Average SA/V ± Std.	Diameter calculated from SA/V
Isolated (pH 5.8)	1	9.42×10^{-6}	2.03×10^{-5}	0.732	0.46	0.40 ± 0.04	15.0 ± 1.5
	2	1.40×10^{-5}	3.60×10^{-5}	0.740	0.39		
	3	1.30×10^{-5}	3.50×10^{-5}	0.739	0.37		
	4	1.25×10^{-5}	3.18×10^{-5}	0.737	0.39		
Acid-aggregated (pH 2.6)	1	1.19×10^{-6}	2.25×10^{-5}	0.908	0.053	0.046 ± 0.005	130 ± 14
	2	1.12×10^{-6}	2.57×10^{-5}	0.951	0.044		
	3	1.63×10^{-6}	3.65×10^{-5}	0.920	0.045		
	4	3.01×10^{-6}	7.61×10^{-5}	0.951	0.040		
THPC-aggregated (Au:THPC = 62.5) (pH 5.8)	1	8.66×10^{-6}	2.31×10^{-5}	0.731	0.37	0.36 ± 0.02	16.7 ± 1.0
	2	4.15×10^{-6}	1.17×10^{-5}	0.735	0.35		
	3	8.09×10^{-6}	2.15×10^{-5}	0.735	0.37		
	4	1.05×10^{-5}	3.15×10^{-5}	0.741	0.33		

are very similar, with a charge of 20.3 μC, 23.1 μC, and 22.5 μC, respectively, for non-aggregated, THPC-aggregated, and acid-aggregated Au NPs. While they have similar oxidation charge (similar Au V), their SA charge was found to be 9.42 μC, 8.66 μC, and 1.19 μC for the isolated,

THPC-aggregated, and acid-aggregated NPs, respectively. With similar V, the SA was about 7-8 times lower for the acid-aggregated Au NPs compared to the non-aggregated or THPC-aggregated Au NPs.

Table 1 shows all data of isolated, THPC- and acid-aggregated Au NPs. The average SA/V ratio from 4 different samples was 0.40 ± 0.04, 0.36 ± 0.02 and 0.046 ± 0.005, respectively (Table 1, column 7). The measured geometric size, considering that the diameter of a sphere is equal to 6V/SA, corresponds to average diameters of 15.0 ± 1.5 nm, 16.7 ± 1.0 nm, and 130 ± 14 nm, respectively (Table 1, column 8). This result indicates that THPC-aggregated NPs do not lose their electroactive SA, while the SA and SA/V of acid-aggregated NPs decreases dramatically. The large decrease in SA/V is the reason for the large positive shift in E_p for the acid-aggregated NPs. There is a small shoulder at higher potentials in the ASV of the THPC-aggregated NPs (Figure 3B, blue plot), which is consistent with the very small decrease in electrochemically-measured SA/V compared to isolated Au NPs. This is likely due to a small population of THPC-aggregated NPs that had a significant decrease in SA/V. The large decrease in SA/V for acid-aggregated Au NPs is due to the 3D nature of the aggregates and fusion of the Au NPs, as observed in the STEM images. These results show that the ASV is not only sensitive to NP size and aggregation, but also the specific aggregate structural details.

We finally studied the effect of the Au:THPC mole ratio on the the resulting structure of the NP aggregates and measured E_p. Figure 4A shows the UV-vis spectra of 15 nm diameter citrate-stabilized Au NPs with THPC added in Au:THPC mole ratios of 62.5, 31.3, 10.4, and 6.3. The results show very minimal changes in the LSPR band position with this increasing THPC concentration by up to a factor of 10. The absorbance at 700-710 nm slightly decreased, indicating the potential start of NP precipitation, but the spectra are otherwise very similar. Figure 4B shows

Table 2. SA/V determination of THPC-aggregated Au NPs with various Au:THPC molar ratios.

Au:THPC mole ratio	Trial #	CV measured surface area (C)	ASV measured total volume (C)	Peak Oxidation Potential E_p (V) vs Ag/AgCl	Average E_p ± Std. Dev. (V)	Surface area to volume ratio (SA/V)	Average SA/V ± Std. Dev.
62.5	1	8.66×10^{-6}	2.31×10^{-5}	0.731	0.733 ± 0.002	0.37	0.36 ± 0.01
	2	4.15×10^{-6}	1.17×10^{-5}	0.735		0.35	
	3	8.09×10^{-6}	2.15×10^{-5}	0.735		0.37	
31.3	1	4.19×10^{-6}	2.25×10^{-5}	0.789	0.781 ± 0.010	0.19	0.19 ± 0.01
	2	5.15×10^{-6}	2.80×10^{-5}	0.783		0.18	
	3	5.25×10^{-6}	2.67×10^{-5}	0.773		0.20	
10.4	1	3.52×10^{-6}	2.25×10^{-5}	0.828	0.818 ± 0.010	0.16	0.15 ± 0.02
	2	3.54×10^{-6}	2.20×10^{-5}	0.819		0.16	
	3	2.77×10^{-6}	2.07×10^{-5}	0.809		0.13	
6.3	1	4.70×10^{-6}	4.06×10^{-5}	0.882	0.882 ± 0.005	0.12	0.11 ± 0.01
	2	9.72×10^{-7}	1.01×10^{-5}	0.878		0.10	
	3	1.20×10^{-6}	1.25×10^{-5}	0.888		0.10	

ASVs of glass/ITO/APTES electrodes coated with Au NPs aggregated using the same Au:THPC mole ratios used in Figure 4A. With ASV, the E_p shifted incrementally more positive as the amount of THPC added increased. The E_p values for the various ratios were 0.733 ± 0.002 V, 0.781 ± 0.010 V, 0.819 ± 0.010 V, and 0.882 ± 0.005 V vs. Ag/AgCl for Au:THPC mole ratios of 62.5, 31.3 10.4 and 6.3, respectively, as shown in Figure 4B (Table 2). The positive shift in oxidation potential indicates that higher amounts of THPC leads to aggregation in a similar fashion to the 3D assembly and NP fusion observed for acid aggregated Au NPs. In order to compare their SA/V ratios, we compared the SA values for samples that had a very similar ASV coverage as shown in Figure 4C. The electroactive SA decreased with a decrease in Au:THPC mole ratio (increasing THPC). The SA/V ratios were 0.36 ± 0.02, 0.19 ± 0.01, 0.15 ± 0.02 and 0.11 ± 0.01 for Au:THPC mole ratios of 62.5, 31.3, 10.4, and 6.3, respectively (Table 2, column 7). This again shows the correlation between E_p and SA/V of the aggregates formed. The E_p values correlate very well with the SEM and STEM images of the THPC-aggregated Au NPs with varying THPC.

For Au:THPC mole ratio of 62.5, the aggregates were 1D/2D structures with clear ~1 nm gap between the Au NPs (Figure 2E and 4D). For Au:THPC mole ratio of 6.3, most of the NPs were assembled into 3D structures and were interconnected, or fused, as shown in the STEM image of Figure 4E (see red arrows). It is not clear at this time exactly why the larger amount of THPC leads to interconnected, or fused, Au NPs.

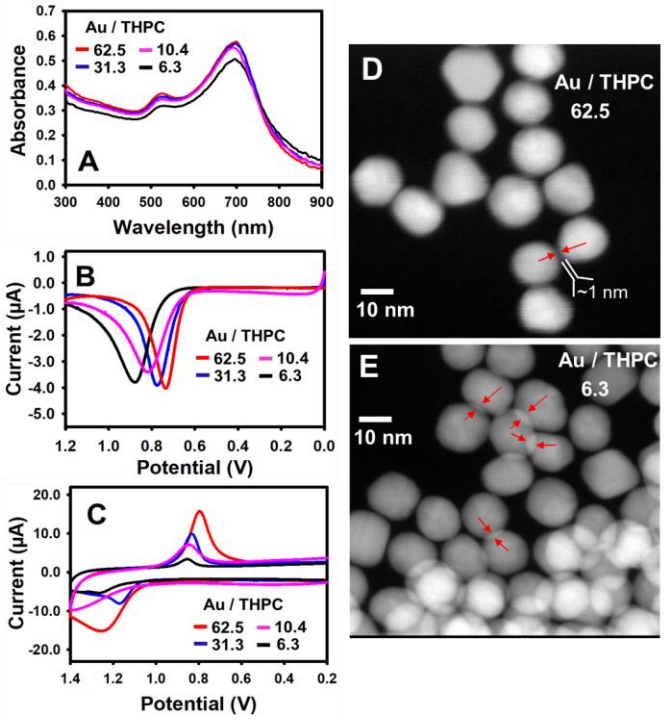

Figure 4. (A) UV−vis spectra of 15 nm diameter Au NP solutions aggregated with various Au:THPC ratios of 62.5 (red graph), 31.3 (blue graph) 10.4 (pink graph) and 6.3 (black graph). (B) ASVs of corresponding aggregated Au NPs from (A) attached to glass/ITO/APTES electrodes performed in 0.1 M $KClO_4$ + 0.01 M KBr from -0.2 to +1.4 V at a scan rate of 10 mV/s (0.0 to 1.2 V is shown). (C) CVs of the corresponding aggregated Au NPs. CVs were performed in 0.1 M $HClO_4$ solutions. (D,E) STEM images of THPC-aggregated NPs with the Au:THPC ratios of 62.5 and 6.3, respectively.

We finally measured the surface charge by monitoring the zeta potential of isolated, acid-aggregated, and THPC-aggregated Au NPs with various Au:THPC mole ratios. The zeta potential was -25 ± 2, and 16 ± 1 mV for isolated and acid-aggregated NPs. The increase of the zeta potential value with the decrease of pH was observed by Diegoli *et. al* previously.[42] However, they only monitored the zeta potential values from pH 5.5 to 3.0 which is not sufficient for complete neutralization of the negative charges of citrate ions. Complete aggregation of citrate-coated Au NPs occurred at pH lower than the pk_{a1} value of citrate (2.9) as observed previously by our group[23] and others.[43] The zeta potential was -47 ± 1, -42 ± 2, -36 ± 4, and -22 ± 4 mV for Au:THPC mole ratios of 62.5, 31.3, 10.4, and 6.3, respectively. The pH of the

corresponding solutions was 5.8, 5.0, 4.6 and 3.6, respectively. The initial decrease in the zeta potential for the Au:THPC mole ratio of 62.5 relative to the original Au NPs is due to the formation of large aggregates and poor NP size uniformity, which is not ideal for zeta potential measurements.[30] The positive increase in zeta potential with increasing THPC is partly due to replacement of the negatively-charged citrate with the positively-charged THPC or neutral pentavalent THPC hydroxide (THPOH), which can be formed by Au NP-catalyzed oxidation of THPC through a tri(hydroxymethyl) phosphine oxide (THPO) intermediate.[30, 42] With an increase in THPC, the pH of the solution also decreases due to acid produced during the conversion of THPC to THPO as reported previously,[44] which likely leads to protonation of citrate and NP fusion as with acid-aggregated Au NPs.

CONCLUSIONS

In conclusion, we showed here that the E_p of 15 nm diameter citrate-stabilized Au NPs depends on whether they are well-isolated, arranged in a 1D/2D aggregated assembly with space between the NPs, or in a 3D aggregate with the NPs interconnected, or fused. The addition of low amounts of THPC (Au:THPC mole ratio = 62.5) led to 1D/2D assemblies with gaps between the aggregated NPs. The addition of acid to lower the NP solution pH below 3 or addition of large amounts of THPC (Au:THPC mole ratio = 6-30) to the Au NPs led to 3D assemblies consisting of interconnected Au NPs. In all 3 cases, the solutions turned purple/blue and the UV-vis showed significant absorbance at higher wavelengths, indicative of plasmonic coupling between the aggregated NPs in the assembly. Interestingly, the E_p of the Au NPs shifted positive relative to isolated Au NPs at low pH and with high amounts of THPC, where the NPs were in a 3D assembly with interconnected NPs. The E_p did not shift with low amounts of THPC, where the aggregated

NPs were in a 1D/2D assembly with ~1 nm gaps between the NPs. The 3D interconnected assemblies showed a significantly lower electrochemically-measured SA/V compared to isolated or 1D/2D NP assemblies with low THPC. The measured SA/V was consistent with the measured E_p, where a lower SA/V led to a higher E_p, consistent with our recent work on Au NPs attached to electrode surfaces by different methods.[33] Zeta potential measurements were consistent with pH neutralization of the NPs or replacement of citrate with THPC during aggregation. Studying the electrochemical properties of aggregated metal nanostructures is important for gaining a better fundamental understanding of metal NP reactivity and for applications in aggregation-based sensors and electrocatalysis. For sensing applications, analyte could be detected by a shift in E_p if the analyte-induced aggregation leads to NP fusion, but undetectable if spacing remains between NPs. For catalysis, NP aggregation with spacing between NPs could lead to high density and high surface area, which could potentially be beneficial for many electrocatalytic application.

AUTHOR INFORMATION

Corresponding Author

*E-mail: f.zamborini@louisville.edu

Author Contributions

†D.K.P and H.N.N contributed equally.

Notes

The authors declare no competing financial interest.

ACKNOWLEDGMENTS

We gratefully acknowledge the National Science Foundation (NSF) for financial support of this research through grants CHE-1611170 and CHE-2004169.

SUPPORTING INFORMATION

Digital pictures of non-aggregated and aggregated Au NPs are in the supporting information.

REFERENCES

1. Trindell, J. A.; Clausmeyer, J.; Crooks, R. M., Size Stability and H_2/CO Selectivity for Au Nanoparticles during Electrocatalytic CO_2 Reduction. *J. Am. Chem. Soc.* **2017,** *139*, 16161-16167.
2. Busbee, B. D.; Obare, S. O.; Murphy, C. J., An Improved Synthesis of High-Aspect-Ratio Gold Nanorods. *Adv. Mater.* **2003,** *15*, 414-416.
3. Rai, A.; Singh, A.; Ahmad, A.; Sastry, M., Role of Halide Ions and Temperature on the Morphology of Biologically Synthesized Gold Nanotriangles. *Langmuir* **2006,** *22*, 736-741.
4. Pattadar, D. K.; Zamborini, F. P., A Size Stability Study of Catalytically-Active Sub-2 nm Diameter Gold Nanoparticles Synthesized with Weak Stabilizers. *J. Am. Chem. Soc.* **2018,** *140*, 14126-14133.
5. Manthiram, K.; Surendranath, Y.; Alivisatos, A. P., Dendritic Assembly of Gold Nanoparticles during Fuel-Forming Electrocatalysis. *J. Am. Chem. Soc.* **2014,** *136*, 7237-7240.
6. Jassby, D.; Farner Budarz, J.; Wiesner, M., Impact of Aggregate Size and Structure on the Photocatalytic Properties of TiO_2 and ZnO Nanoparticles. *Environ. Sci. Technol.* **2012,** *46*, 6934-6941.
7. Liu, L.; Corma, A., Metal Catalysts for Heterogeneous Catalysis: From Single Atoms to Nanoclusters and Nanoparticles. *Chem. Rev.* **2018,** *118*, 4981-5079.
8. Feng, J.-J.; Guo, H.; Li, Y.-F.; Wang, Y.-H.; Chen, W.-Y.; Wang, A.-J., Single Molecular Functionalized Gold Nanoparticles for Hydrogen-Bonding Recognition and Colorimetric Detection of Dopamine with High Sensitivity and Selectivity. *ACS App. Mater. Interfaces* **2013,** *5*, 1226-1231.
9. Daniel, W. L.; Han, M. S.; Lee, J.-S.; Mirkin, C. A., Colorimetric Nitrite and Nitrate Detection with Gold Nanoparticle Probes and Kinetic End Points. *J. Am. Chem. Soc.* **2009,** *131*, 6362-6363.
10. Lee, J.-S.; Ulmann, P. A.; Han, M. S.; Mirkin, C. A., A DNA−Gold Nanoparticle-Based Colorimetric Competition Assay for the Detection of Cysteine. *Nano Lett.* **2008,** *8*, 529-533.
11. Elghanian, R.; Storhoff, J. J.; Mucic, R. C.; Letsinger, R. L.; Mirkin, C. A., Selective Colorimetric Detection of Polynucleotides Based on the Distance-Dependent Optical Properties of Gold Nanoparticles. *Science* **1997,** *277*, 1078-1081.
12. Hurst, S. J.; Han, M. S.; Lytton-Jean, A. K. R.; Mirkin, C. A., Screening the Sequence Selectivity of DNA-Binding Molecules Using a Gold Nanoparticle-Based Colorimetric Approach. *Anal. Chem.* **2007,** *79*, 7201-7205.
13. Lee, A.; Andrade, G. F. S.; Ahmed, A.; Souza, M. L.; Coombs, N.; Tumarkin, E.; Liu, K.; Gordon, R.; Brolo, A. G.; Kumacheva, E., Probing Dynamic Generation of Hot-Spots in Self-Assembled Chains of Gold Nanorods by Surface-Enhanced Raman Scattering. *J. Am. Chem. Soc.* **2011,** *133*, 7563-7570.

14. Izquierdo-Lorenzo, I.; Kubackova, J.; Manchon, D.; Mosset, A.; Cottancin, E.; Sanchez-Cortes, S., Linking Ag Nanoparticles by Aliphatic α,ω-Dithiols: A Study of the Aggregation and Formation of Interparticle Hot Spots. *J. Phys. Chem. C* **2013,** *117*, 16203-16212.
15. Dasari, R.; Zamborini, F. P., Surface Enhanced Raman Spectroscopy at Electrochemically Fabricated Silver Nanowire Junctions. *Anal. Chem.* **2016,** *88*, 675-681.
16. Wei, Y.; Han, S.; Kim, J.; Soh, S.; Grzybowski, B. A., Photoswitchable Catalysis Mediated by Dynamic Aggregation of Nanoparticles. *J. Am. Chem. Soc.* **2010,** *132*, 11018-11020.
17. Lu, Q.; Huang, J.; Han, C.; Sun, L.; Yang, X., Facile Synthesis of Composition-Tunable PtRh Nanosponges for Methanol Oxidation Reaction. *Electrochimica Acta* **2018,** *266*, 305-311.
18. Wen, D.; Liu, W.; Haubold, D.; Zhu, C.; Oschatz, M.; Holzschuh, M.; Wolf, A.; Simon, F.; Kaskel, S.; Eychmüller, A., Gold Aerogels: Three-Dimensional Assembly of Nanoparticles and Their Use as Electrocatalytic Interfaces. *ACS Nano* **2016,** *10*, 2559-2567.
19. Cai, B.; Wen, D.; Liu, W.; Herrmann, A.-K.; Benad, A.; Eychmüller, A., Function-Led Design of Aerogels: Self-Assembly of Alloyed PdNi Hollow Nanospheres for Efficient Electrocatalysis. *Angew. Chem.* **2015,** *54*, 13101-13105.
20. Vilela, D.; González, M. C.; Escarpa, A., Sensing Colorimetric Approaches Based on Gold and Silver Nanoparticles Aggregation: Chemical Creativity Behind the Assay. A Review. *Anal. Chim. Acta* **2012,** *751*, 24-43.
21. Baalousha, M.; Nur, Y.; Römer, I.; Tejamaya, M.; Lead, J. R., Effect of Monovalent and Divalent Cations, Anions and Fulvic Acid on Aggregation of Citrate-Coated Silver Nanoparticles. *Sci. Total Environ* **2013,** *454-455*, 119-131.
22. Sun, L.; Song, Y.; Wang, L.; Guo, C.; Sun, Y.; Liu, Z.; Li, Z., Ethanol-Induced Formation of Silver Nanoparticle Aggregates for Highly Active SERS Substrates and Application in DNA Detection. *J. Phys. Chem. C* **2008,** *112*, 1415-1422.
23. Allen, S. L.; Sharma, J. N.; Zamborini, F. P., Aggregation-Dependent Oxidation of Metal Nanoparticles. *J. Am. Chem. Soc.* **2017,** *139*, 12895-12898.
24. Cloake, S. J.; Toh, H. S.; Lee, P. T.; Salter, C.; Johnston, C.; Compton, R. G., Anodic Stripping Voltammetry of Silver Nanoparticles: Aggregation Leads to Incomplete Stripping. *ChemistryOpen* **2015,** *4*, 22-26.
25. He, D.; Bligh, M. W.; Waite, T. D., Effects of Aggregate Structure on the Dissolution Kinetics of Citrate-Stabilized Silver Nanoparticles. *Environ. Sci. & Technol.* **2013,** *47*, 9148-9156.
26. Rees, N. V.; Zhou, Y.-G.; Compton, R. G., The Aggregation of Silver Nanoparticles in Aqueous Solution Investigated via Anodic Particle Coulometry. *ChemPhysChem* **2011,** *12*, 1645-1647.
27. Pattadar, D. K.; Sharma, J. N.; Mainali, B. P.; Zamborini, F. P., Anodic Stripping Electrochemical Analysis of Metal Nanoparticles. *Curr. Opin. Electrochem.* **2019,** *13*, 147-156.
28. Tschulik, K.; Batchelor-McAuley, C.; Toh, H.-S.; Stuart, E. J. E.; Compton, R. G., Electrochemical Studies of Silver Nanoparticles: a Guide for Experimentalists and a Perspective. *Phys. Chem. Chem. Phys.* **2014,** *16*, 616-623.
29. Turkevich, J.; Stevenson, P. C.; Hillier, J., A Study of the Nucleation and Growth Processes in the Synthesis of Colloidal Gold. *Discuss. Faraday Soc.* **1951,** *11*, 55-75.
30. Gulka, C. P.; Wong, A. C.; Wright, D. W., Spontaneous Self-Assembly and Disassembly of Colloidal Gold Nanoparticles Induced by Tetrakis(hydroxymethyl) Phosphonium Chloride. *Chem. Commun.* **2016,** *52*, 1266-1269.
31. Pattadar, D. K.; Zamborini, F. P., Effect of Size, Coverage, and Dispersity on the Potential-Controlled Ostwald Ripening of Metal Nanoparticles. *Langmuir* **2019,** *35*, 16416-16426.

32. Pattadar, D. K.; Masitas, R. A.; Stachurski, C. D.; Cliffel, D. E.; Zamborini, F. P., Reversing the Thermodynamics of Galvanic Replacement Reactions by Decreasing the Size of Gold Nanoparticles. *J. Am. Chem. Soc.* **2020,** *142*, 19268-19277.
33. Sharma, J. N.; Pattadar, D. K.; Mainali, B. P.; Zamborini, F. P., Size Determination of Metal Nanoparticles Based on Electrochemically Measured Surface Area-to-Volume Ratio. *Anal. Chem.* **2018,** *90*, 9308-9314.
34. Nam, J.; Won, N.; Jin, H.; Chung, H.; Kim, S., pH-Induced Aggregation of Gold Nanoparticles for Photothermal Cancer Therapy. *J. Am. Chem. Soc.* **2009,** *131*, 13639-13645.
35. Zhang, H.; Fung, K.-H.; Hartmann, J.; Chan, C. T.; Wang, D., Controlled Chainlike Agglomeration of Charged Gold Nanoparticles via a Deliberate Interaction Balance. *J. Phys. Chem. C* **2008,** *112*, 16830-16839.
36. Liu, X.; Xu, H.; Xia, H.; Wang, D., Rapid Seeded Growth of Monodisperse, Quasi-Spherical, Citrate-Stabilized Gold Nanoparticles via H_2O_2 Reduction. *Langmuir* **2012,** *28*, 13720-13726.
37. Pattadar, D. K.; Mainali, B. P.; Jasinski, J. B.; Zamborini, F. P., Electrooxidation, Size Stability, and Electrocatalytic Activity of 0.9 nm Diameter Gold Nanoclusters Coated with a Weak Stabilizer. *ChemElectroChem* **2020,** *7*, 800-809.
38. Demers, S. M. E.; Hsieh, L. J. H.; Shirazinejad, C. R.; Garcia, J. L. A.; Matthews, J. R.; Hafner, J. H., Ultraviolet Analysis of Gold Nanorod and Nanosphere Solutions. *J. Phys. Chem. C* **2017,** *121*, 5201-5207.
39. Shajari, D.; Bahari, A.; Gill, P.; Mohseni, M., Synthesis and Tuning of Gold Nanorods with Surface Plasmon Resonance. *Opt. Mater.* **2017,** *64*, 376-383.
40. Pattadar, D. K.; Sharma, J. N.; Mainali, B. P.; Zamborini, F. P., Impact of the Assembly Method on the Surface Area-to-Volume Ratio and Electrochemical Oxidation Potential of Metal Nanospheres. *J. Phys. Chem. C* **2019,** *123*, 24304-24312.
41. Mainali, B. P.; Pattadar, D. K.; Zamborini, F. P., Size-Dependent Ripening of Gold Nanoparticles through Repetitive Electrochemical Surface Oxidation-Reduction Cycling. *J. Electrochem. Soc.* **2020,** *167*, 146503.
42. Diegoli, S.; Mendes, P. M.; Baguley, E. R.; Leigh, S. J.; Iqbal, P.; Garcia Diaz, Y. R.; Begum, S.; Critchley, K.; Hammond, G. D.; Evans, S. D.; Attwood, D.; Jones, I. P.; Preece, J. A., pH-Dependent Gold Nanoparticle Self-Organization on Functionalized Si/SiO_2 Surfaces. *J. Exp. Nanosci* **2006,** *1*, 333-353.
43. Li, X.; Tamada, K.; Baba, A.; Hara, M., pH-Controlled Two Dimensional Gold Nanoparticle Aggregates for Systematic Study of Local Surface Plasmon Coupling. *J. Nanosci. Nanotechnol.* **2009,** *9*, 408-416.
44. Mateo, J. M.; Hoz, A. d. l.; Usón, L.; Arruebo, M.; Sebastian, V.; Gomez, M. V., Insights into the Mechanism of the Formation of Noble Metal Nanoparticles by In Situ NMR Spectroscopy. *Nanoscale Adv.* **2020,** *2*, 3954-3962.

TOC FIGURE